Fully reprogrammable 2D array of multistate molecular switching units

Anja Bauer, Tobias Birk, Fabian Paschke, Andreas Fuhrberg, Josefine Diegel, Ann Kathrin Becherer, Lars Vogelsang, Markus Maier, Werner M. Schosser, Fabian Pauly, Oded Zilberberg, Rainer F. Winter, Mikhail Fonin

Fully Reprogrammable 2D Array of Multistate Molecular Switching Units

*Anja Bauer, Tobias Birk, Fabian Paschke, Andreas Fuhrberg, Josefine Diegel,
Ann-Kathrin Becherer, Lars Vogelsang, Markus Maier, Werner M. Schosser, Fabian Pauly,
Oded Zilberberg, Rainer F. Winter, and Mikhail Fonin**

Integration of molecular switching units into complex electronic circuits is considered to be the next step toward the realization of novel logic and memory devices. This paper reports on an ordered 2D network of neighboring ternary switching units represented by triazatruxene (TAT) molecules organized in a honeycomb lattice on a Ag(111) surface. Using low-temperature scanning tunneling microscopy, the bonding configurations of individual TAT molecules can be controlled, realizing up to 12 distinct states per molecule. The switching between those states shows a strong bias dependence ranging from tens of millivolts to volts. The low-bias switching behavior is explored in active units consisting of two and more interacting TAT molecules that are purposefully defined (programmed) by high-bias switching within the honeycomb lattice. Within such a unit the low-bias switching can be triggered and accessed by single-point measurements on a single TAT molecule, demonstrating up to 9 and 19 distinguishable states in a dyad and a tetrad of coupled molecules, respectively. High experimental control over the desired state, owing to bias-dependent hierarchical switching and pronounced switching directionality, as well as full reversibility, make this system particularly appealing, paving the way to design complex molecule-based memory systems.

1. Introduction

Electronic devices based on functional molecular units may outperform traditional silicon-based electronic components,

thus providing an ultimate solution for high-density logic and memory units.[1–6] In this regard, molecular switches are supposed to play a central role, owing to the possibility of controllably toggling the system between two or more stable states.[7–9] To harvest the switching property for logic or memory applications,[4–6] molecules are usually contacted to electrodes giving a possibility of electrical manipulation as well as read-out. Experimental realization on the single molecule scale relies on two main approaches:[4] First, the switching behavior is studied in molecular transport devices; second, the switching behavior is probed by scanning tunneling microscopy (STM). Implementation of the latter technique allows to address the molecular systems in well-controlled geometries and has recently provided profound insights into proof-of-concept building blocks based on the rotational motion of molecules,[10–19] on their charge states,[20–24] on intramolecular atom transfer,[25–34] on conformational changes,[35–38] on formation and dissociation of chemical bonds,[39–42] and on spin-state switching.[43–48]

Although the vast majority of experimental work has been done on bistable molecules, multistate systems[49,50] are

A. Bauer, T. Birk, F. Paschke[+], A. Fuhrberg, J. Diegel, A.-K. Becherer,
O. Zilberberg, M. Fonin[+]
Fachbereich Physik
Universität Konstanz
78457 Konstanz, Germany
E-mail: mikhail.fonin@uni-konstanz.de

The ORCID identification number(s) for the author(s) of this article can be found under https://doi.org/10.1002/adma.202401662

[+]Present address: IBM Research Europe – Zurich, Rüschlikon 8803, Switzerland

L. Vogelsang, M. Maier, R. F. Winter
Fachbereich Chemie
Universität Konstanz
78457 Konstanz, Germany
W. M. Schosser, F. Pauly
Institute of Physics and Centre for Advanced Analytics and Predictive Sciences
University of Augsburg
86159 Augsburg, Germany

**ADVANCED
SCIENCE NEWS**

www.advancedsciencenews.com

**ADVANCED
MATERIALS**

www.advmat.de

particularly appealing, as they would allow to increase the surface unit density and simultaneously reduce the circuit complexity. However, single-molecule multistate systems are less explored and only recently, transport-device-related examples started to emerge.[51–53] With regard to on-surface molecular systems studied by STM, reports exist on three-state switching in a spin–crossover complex,[48] three-level switching between equivalent bonding configurations,[54,55] four-level switches based on tautomerization,[27,33] three-,[49] five-[14] and six-step[13,17] molecular rotors, as well as on hierarchical six-level switching owing to the core rotation in Cs$_3$N@C$_{80}$[56] and on 14-level adsorption configuration switching of Li@C$_{60}$.[57]

Here, we present a study of multistate hierarchical switching within an ordered 2D network of *N,N′,N″*-triethyltriazatruxene (TAT) molecules on Ag(111). By means of STM, we are able to reversibly manipulate the binding configurations of individual TAT molecules within the dense molecular layer. The interconversion between three bonding types using high-bias voltage pulses combined with additional bonding configurations within each of these types allows us to realize 12 distinct states per molecule. We further explore the control over the final state by relying on switching hierarchy and directionality. Based on these thorough characterizations, we are able to define switching units within the lattice consisting of two or more interacting molecules that show low-bias switching, and investigate their switching dynamics.
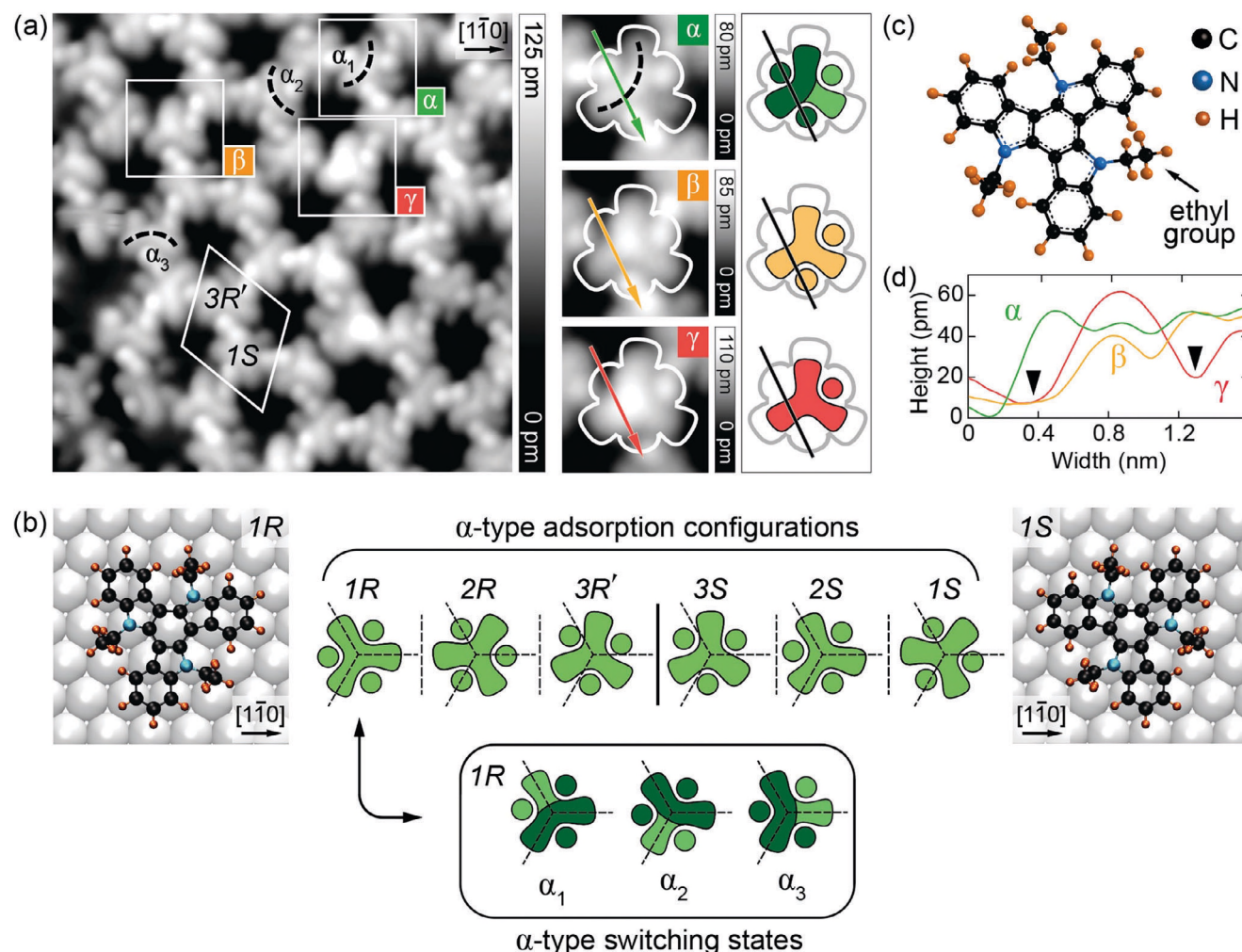
2. Results and Discussion

Surface deposition of TAT was performed by the electrospray method[58,59] (see Figure S1, Supporting Information) with the Ag(111) substrate kept at room temperature. In **Figure 1a**, we show a low-temperature STM image of a well-ordered honeycomb lattice within an island of TAT molecules on Ag(111). This structure is usually obtained at coverages exceeding approximately half of a close-packed molecular layer (see Figure S2). The majority of TAT molecules within the honeycomb lattice exhibit a distinct shape reflecting the trigonal symmetry of the molecular structure, giving the possibility to exactly distinguish between different adsorption configurations and binding types.[54]

We first focus on the different adsorption geometries of TAT on Ag(111) as observed in STM imaging, followed by an analysis of their switching behavior. Upon adsorption, two chiral configurations of the TAT molecule can occur, which are labeled as *R* and *S*. The honeycomb lattice consists of equal numbers of the two surface enantiomers, yielding an ordered racemic mixture (Figure 1a), comparable to other molecular systems.[60] For free-standing molecules, we previously observed two adsorption configurations – 1) *atop-fcc*, and 2) *atop-hcp* (see Figure 1b and Figure S3, Supporting Information), meaning that the central benzene ring of the molecule is placed above an Ag atom (*atop*) and the three attached pyrrole rings are placed above *fcc* or *hcp* hollow sites.[54] The honeycomb lattice stabilizes a third adsorption geometry (labeled as *3S* and *3R′*), where the central benzene ring is proposed to adsorb above an *atop* position (*3S*) or an *hcp*-hollow position (*3R′*), whereas the pyrrole rings are placed above *bridge* positions (see Figure S4, Supporting Information). All configurations can be well identified and distinguished by the molecular rotation with respect to the [1$\bar{1}$0] direction of Ag(111),

as obtained in STM imaging. According to the introduced labeling, the honeycomb lattice shown in Figure 1a is composed of *1S* and *3R′* molecules, thus, yielding the *1S/3R′* configuration. The *3S/1R* configuration was also observed (for details see Figure S4, Supporting Information).

Within every adsorption configuration, TAT molecules can be further classified into three types owing to their STM shape appearance, which we refer to as *α*, *β*, and *γ* bonding types (see boxed areas and corresponding magnifications in Figure 1a). As previously reported,[54,55] the most abundant TAT type is characterized by three prominent circular protrusions (further also referred to as intensity maxima) that surround a three-blade propeller. This appearance will be further referred to as *α*-type. The three intensity maxima represent the *N*-bonded ethyl groups that protrude upwards from the surface, and the propeller-shaped intensity stems from the molecular backbone (see Figure 1b,c). Because of the trigonal symmetry, three equivalent bonding states *α$_i$* (*α$_1$*, *α$_2$*, *α$_3$*) exist within the same adsorption geometry shown in Figure 1b. They can be distinguished in STM by the orientation of the boomerang-shaped intensity distribution of the molecular backbone (see dashed lines in Figure 1a). In free-standing *α*-type TAT molecules, a switching between the three states *α$_i$* can be reliably induced upon application of bias voltages in the range of 50–100 mV (low-bias switching).[54] This type, thus, lays the foundation for a trit (ternary digit)-based molecular unit. *β*- and *γ*-type TAT are characterized by molecular shapes with only two and one pronounced maxima visible, respectively, contrary to the *α*-type, which shows three pronounced maxima. As will be shown in the following, the molecular types differ by the number of ethyl groups that are strongly bound to the surface – 0 for *α*-type, 1 for *β*-type, and 2 for *γ*-type molecules. These bonding differences lead to the lack of one (*β*-type) or two (*γ*-type) intensity maxima in STM images (see line profiles in Figure 1d), as compared to the *α*-type. Upon application of voltage ramps up to 2.0–2.6 V over TAT molecules, we are able to initiate reversible transitions between the types without any notable changes in their lateral position as shown in **Figure 2**. In particular, a conversion sequence *α → β → γ* of a *3S*-TAT molecule is presented in Figure 2a together with the inverse conversion sequence (*γ → β → α*) displayed in Figure 2b.

In all experiments presented here, the STM tip was positioned either above the center of the molecule for the switching of *α*-type or in proximity to the missing intensity maximum in the cases of *β*- and *γ*-type molecules. Interestingly, for the *β*-type molecule, we were also able to switch between the three equivalent adsorption configurations (see Figure 2c). This *β$_1$ → β$_2$ → β$_3$* conversion is subject to a pronounced switching directionality, which allows for a high degree of control over the desired final state (see Figure 2c and Figure S5, Supporting Information). Sorted by the initial state of *3S*-TAT, the switching probabilities are shown in Figure 2d. Each attempt represents a voltage ramp from 2.0 to 2.6 V with a ramp rate of 0.2 V/s. The switching probability is defined by the number of successful attempts (switching event occurs) divided by the total number of attempts. For transitions between *α*- and *β*-type the probability amounts to about 44%, whereas the switching probability between the three energetically degenerate *β*-type configurations is about 33%. The probability for transitions into *γ*-type starting from *α*- or *β*-type is about 3%. On the other hand, the transition probability for *γ → α, β* is close

ADVANCED
SCIENCE NEWS
www.advancedsciencenews.com

**ADVANCED
MATERIALS**
www.advmat.de

Figure 1. Honeycomb lattice of TAT on Ag(111). a) Topographic STM image of a TAT island (9.5 × 9.5 nm^2; $I = 100$ pA; $U = 20$ mV). The unit cell (white rhombus) consists of two TAT enantiomers adsorbed in different geometries – *1S* and *3R′*. Three molecular types (α, β, and γ) within the *3R′* configuration are marked by boxes. Magnifications (2 × 2 nm^2) of the boxed TAT molecules are shown on the right-hand side. Pictograms for each TAT type are introduced, which depicts the STM intensity distribution. Filled circles represent the bright circular protrusions in the STM, corresponding to the upstanding ethyl groups. Black lines denote the height profiles. b) Upper row: top views of the adsorption configurations of two surface enantiomers (*1S* - calculated geometry[54] and *1R* - schematic representation) observed for free-standing α-type TAT molecules. Additionally, schematic representations of six different adsorption configurations for the α-type TAT molecule observed in the experiments are shown. Adsorption configurations *3R′* and *3S* are not exactly mirror symmetric as discussed in the text. Bottom row: schematic representation of the three degenerate bonding states exemplarily presented for the *1R* α-type TAT (α_1, α_2, and α_3), which can be distinguished by the different orientation of the characteristic boomerang-shaped feature indicated by the dark-shaded area within the molecular backbone (marked by dashed bows in "a"). Height differences of the three maxima of single α-type TAT molecule[54] are highlighted by light and dark green. c) Molecular structure of the TAT molecule. The ethyl groups are pointing out of the plane. d) Height profiles along the green (α-type), yellow (β-type), and red (γ-type) arrows shown in "a". Black triangles denote the positions of strongly bound ethyl groups in β- and γ-type TAT molecules.

to 100% (in 13 attempts). The measured values represent a lower boundary, as the switching probability grows with increasing duration of applied high-bias voltage. We note that the observed switching makes it difficult to perform dI/dU spectroscopy on the molecules (see Figure S6, Supporting Information). The spectra obtained for free-standing α- and β-type molecules show a rather flat curve with an increase of the intensity toward +2 V, indicating the proximity of the lowest unoccupied molecular orbital.[54] However, the spectra of α- and β-type molecules are very similar, making it difficult to rely on dI/dU spectroscopy for the identification of molecular types.

We turn to elucidate the nature of the different TAT types, first focusing on the free-standing β-type molecule. In **Figure 3a**, we show an STM image of a β-type *1S*-TAT, characterized by a complete suppression of the STM intensity on one of the three bright circular protrusions as compared with the α-type TAT. As shown above, the electric field of the STM tip can be used to reversibly switch between different types, indicating that the molecular structure remains intact upon switching. We, thus, infer that only the adsorption configuration changes, mostly owing to an altered conformation of the alkyl moieties. Relying on previous reports addressing the interaction of ethyl moieties with metallic

**ADVANCED
SCIENCE NEWS**

www.advancedsciencenews.com

**ADVANCED
MATERIALS**

www.advmat.de
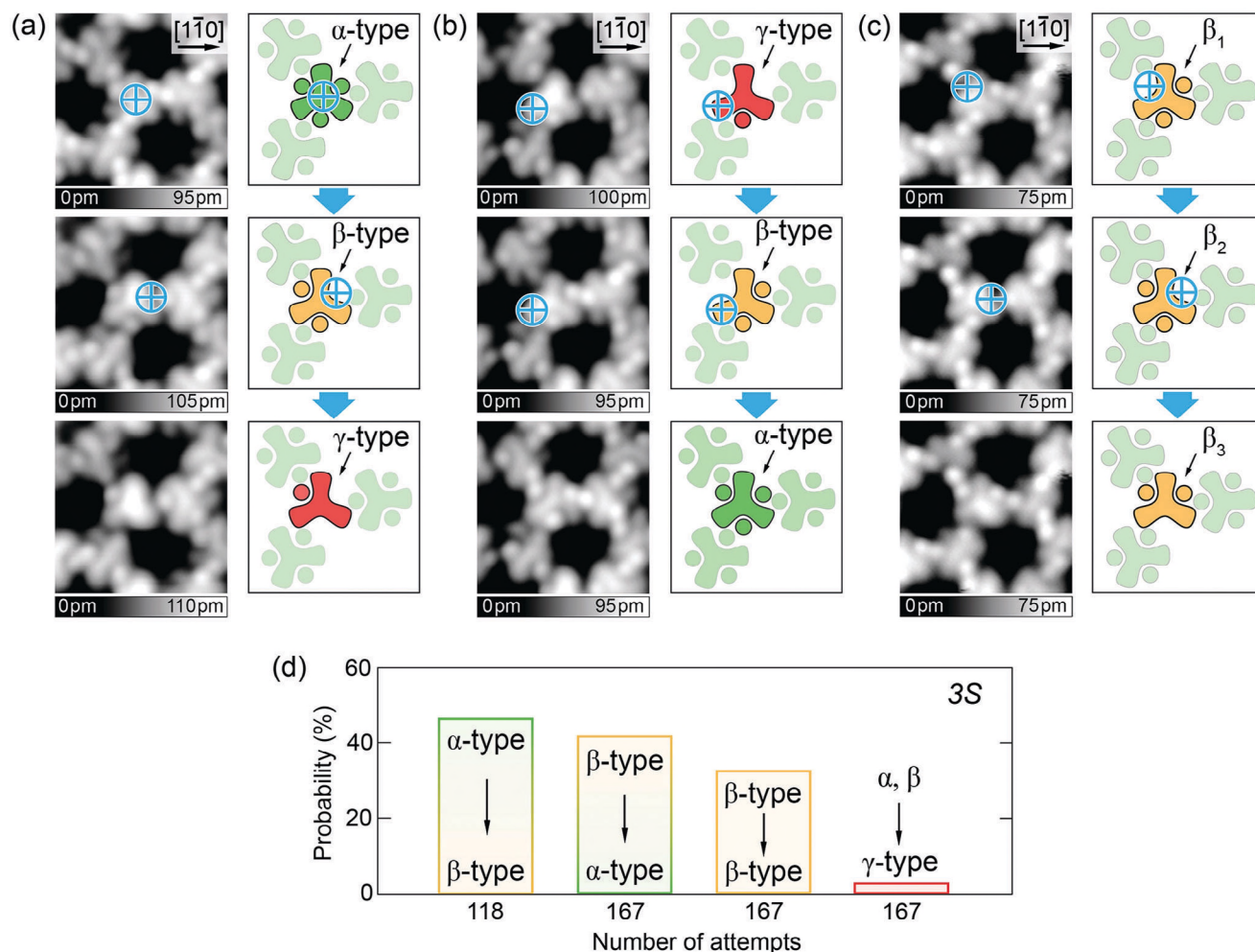
Figure 2. Tip-induced conformational changes of TAT. a) Topographic STM images (left) and corresponding pictograms (right) illustrating tip-induced switching sequences between three different conformations of the central *3S*-TAT molecule: $\alpha \rightarrow \beta \rightarrow \gamma$. b) Inverse switching sequence for the same molecule: $\gamma \rightarrow \beta \rightarrow \alpha$. c) Tip-induced changes between three degenerate ground states of the β-type TAT molecule. All images: 4×4 nm^2; $U = 20$ mV; $I = 100$ pA. The lateral tip positions for each bias ramp are marked by blue crosses in the STM images and pictograms. Number of attempts for a successful switching event: (a) 1, 1; (b) 1, 1; (c) 1, 1. d) Probability histogram for tip-induced switching between the types. Ramping parameters for all experiments: voltage range: 2.0 - 2.6 V; ramp speed: 0.2 V/s; $I = 500$ pA.

surfaces,[18,61–63] we assume that in the α-type TAT molecules, all ethyl groups are protruding from the surface, whereas in β-type TAT one ethyl group resides substantially closer to the Ag(111) surface (labeled as *surface-bound ethyl*, SBE).

This scenario is confirmed by density functional theory (DFT) calculations performed upon variation of the distance between one ethyl moiety and the Ag(111) substrate (see Experimental Section). In addition to the α-type configuration (all ethyl moieties pointing up), the calculations reveal an additional adsorption energy minimum. Here, the vertical distance z of the C2-atom (the methyl carbon atom within the ethyl moiety) to the surface plane amounts to $z_{C2}^{\beta\text{-type}} = 3.89$ Å, being on the same level as the corresponding N-atom (denoted N2 in Figure 3b,c). The distance of N2 to the surface is now slightly larger compared with that of the α-type ($z_{N2}^{\alpha\text{-type}} = 3.62$ Å). The same holds for another nitrogen atom (denoted as N1), which is slightly lifted due to the pinning of the SBE moiety. This uplifting of N1 and N2 results

in a tilting of the whole molecule. This in turn pushes the ethyl group at N1 further away from the surface plane compared with the others, which explains the intensity difference of the two maxima observed in the β-type molecule in STM (Figure 3a). The charge density differences shown in Figure 3e,f suggest an increased charge redistribution at N2 due to the C2-Ag pinning. As a result, the binding energy $E_B^{\beta\text{-type}} = -E_{TAT/Ag} + E_{TAT} + E_{Ag}$ amounts to 2.53 eV per molecule, which represents a strong increase compared with that of 1.05 eV per molecule of the α-type.[54]

We infer that the same holds for the observed shape of the γ-type TAT molecule. In this case, two ethyl moieties are supposed to be pinned to the substrate with only one circular protrusion visible in STM images, which results from the remaining upstanding ethyl group (see Figure 1a). We note that no further types, e.g., with three surface bound ethyl groups, were observed. An increased binding energy between the molecule and the

**ADVANCED
SCIENCE NEWS**

www.advancedsciencenews.com

**ADVANCED
MATERIALS**

www.advmat.de
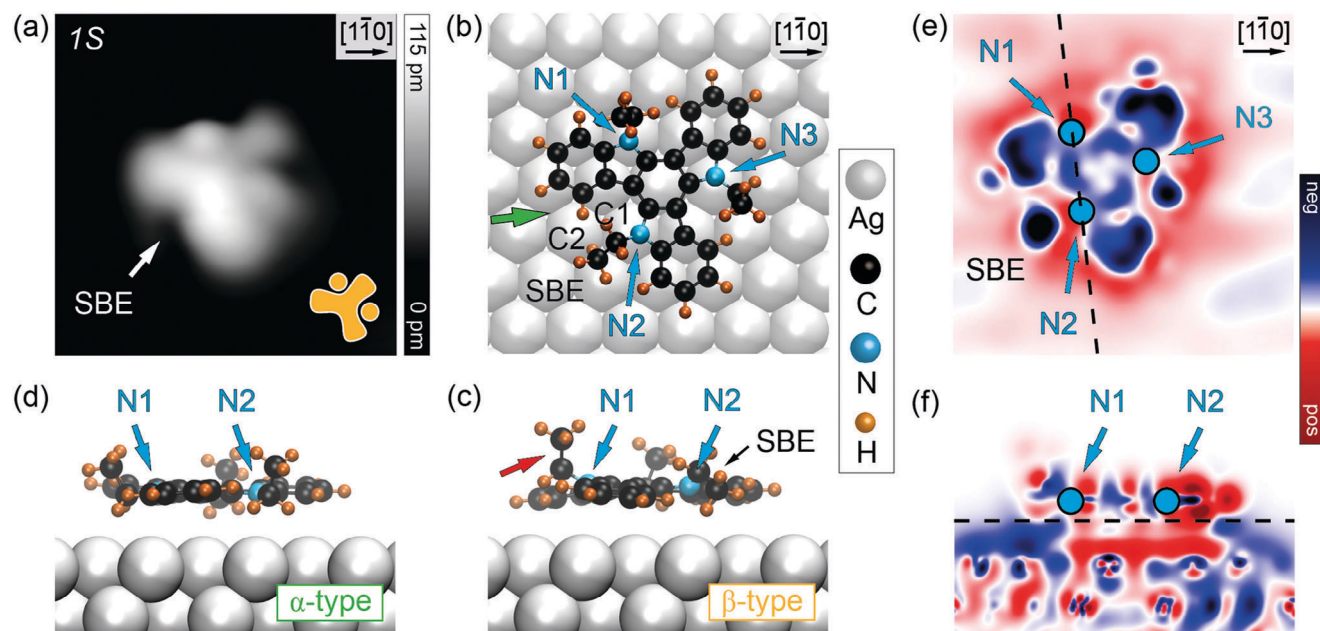
Figure 3. Adsorption geometry of a β-type TAT molecule. a) Topographic STM image of a free-standing β-type *1S*-TAT on Ag(111) (3 × 3 nm²; U = 10 mV; I = 100 pA). One of the bright circular protrusions associated with upstanding ethyl moieties is not visible (SBE: surface-bound ethyl). The corresponding pictogram for the β-type TAT is shown in the lower right corner. b,c) Top- and side-views of the DFT relaxed structure of β-type *1S*-TAT on Ag(111). d) Side view of the DFT relaxed structure of α-type *1S*-TAT on Ag(111) is shown for comparison. The view direction for "c" and "d" is marked in "b" by a green arrow. In the β-type TAT, the ethyl moiety attached to N2 is flipped down toward the Ag(111) surface. The remaining two ethyls are flipped upwards compared with the α-type TAT molecule (a red arrow denotes the highest protruding one). e–f) Charge–density difference calculated as $\Delta\rho(r)$ = $\rho_{TAT/Ag}(r) - \rho_{Ag}(r) - \rho_{TAT}(r)$ and plotted for the geometry shown in "b" and "c". Signs are chosen such that a positive charge or missing electrons are counted as positive. The color scale ranges from $-4\,e/nm^3$ (blue) to $+4\,e/nm^3$ (red), where $e = |e|$ is the elementary charge. Cut plane positions are denoted by dashed lines in "e" and "f".

surface for β- and γ-type molecules is further validated by scanning at elevated bias voltages (0.3–0.7 V), which reveals frequent tip-induced displacements of the α-type molecules, whereas β- and γ-type molecules reside in their adsorption positions (see Figure S7, Supporting Information).

The pinning of the ethyl moieties has a profound effect on the low-bias switching behavior of TAT, as shown for free-standing molecules in **Figure** 4a. A characteristic time trace of the relative tip height, Δz, clearly reflects switching between three degenerate adsorption states in α-type TAT.[54] For β-type
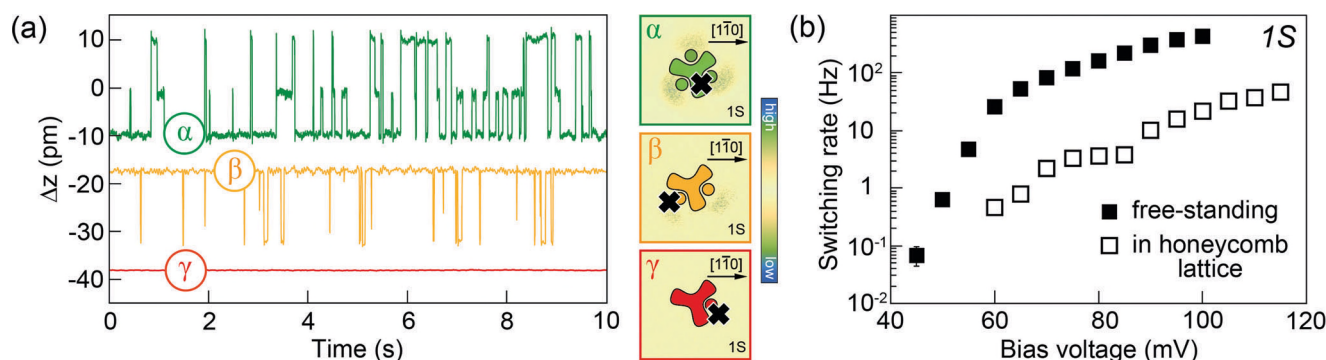
Figure 4. Low-bias switching behavior of TAT molecules. a) $\Delta z(t)$-traces of the relative tip height Δz (drift-corrected) measured on three free-standing TAT molecules (α and γ: U = 50 mV; I = 500 pA; β: U = 10 mV, I = 500 pA). The time traces are vertically shifted for clarity. α-type TAT switches between three states owing to three degenerate bonding configurations within the same adsorption geometry. β-type shows a two-state switching. For γ-type, the low-bias switching is completely suppressed. Tunneling current images on the right show current fluctuations for α and β. No current fluctuations are observed for the γ-type. The color scale ranges from −50 to +50 pA for α, and −15 to +15 pA for β and γ. Imaging parameters: 3 × 3 nm²; U = 200 mV; I = 500 pA. Time-dependent measurements of Δz are performed at the tip positions marked by crosses. b) Switching rate of a free-standing α-type TAT molecule (adapted from Ref. [54]) and of one embedded in the honeycomb lattice (I = 100 pA). Both molecules are in *1S* configuration.

molecules, we observe a two-level switching with one state being clearly preferred, as can be inferred from the dwell times. The difference between both configurations manifests itself as a slight variation in the heights of the two visible ethyl groups, whereas the overall appearance remains almost unchanged. In the following, the two configurations will be referred to as β and β'. For γ-type molecules the molecular switching is completely suppressed, supporting the idea of the pinning of two ethyl moieties to the substrate. We emphasize that low-bias switching is also possible, when the TAT is embedded in the honeycomb lattice. In Figure 4b, we compare the switching rates for a free-standing α-type TAT with the embedded one. The data were obtained by counting all single switching events within a recorded $\Delta z(t)$-trace and dividing this number by the corresponding acquisition time. The increased threshold energy for embedded molecules might be caused by a constrained motion due to the presence of three nearest neighbors in close proximity.

The rich switching behavior as described above suggests TAT/Ag(111) to represent a molecular memory medium. The system shows hierarchical switching at different tunneling bias voltages between accurately distinguishable individual states, as summarized in **Figure 5a**. The β-type shows high-bias switching that is subject to a pronounced switching directionality, which allows to gain considerable control over the desired end state. Within each of the three equivalent adsorption states β_1, β_2, and β_3, low-bias two-state switching $\beta\leftrightarrow\beta'$ is observed (Figure 4a), resulting in a total of six states for β-type TATs (Figure 5a). Pronounced switching rates for the $\beta\leftrightarrow\beta'$ transitions are observed already at bias voltages above 5 mV, which helps to discriminate these transitions from other switching processes. As shown in Figure 2c, switching between the three degenerate configurations of β-type can be controllably induced by high-bias pulses, which provides the possibility to realize a highly stable memory unit owing to the large binding energy of this type. Moreover, the energy barrier is sufficiently high to stabilize the system against spontaneous switching induced by thermal fluctuations not only at the temperatures of about 5 K used in our experiments, but also possibly at those exceeding room temperature. Furthermore, the tip-induced switching can be reliably performed with the possibility to precisely access the desired final state due to the observed switching directionality (Figure 2c and Figure S5, Supporting Information).

For γ-type molecules, a basic memory unit with three states can be realized. As this type does not exhibit low-bias switching, only bias voltages starting from about +2.4 V can be used to change the states or transform the molecule into another type. Voltage-induced transitions between the three configurations of the γ-type are only possible via α- and β-types. However, switching probabilities for α, $\beta \rightarrow \gamma$ are quite low (see Figure 2d), which makes the γ-type somewhat less appropriate for the realization of a memory unit. We note that a further increase of the switching bias above 3 V usually leads to a disruption of the molecular layer or to irreversible changes at TAT molecules, i.e., ethyl detachment (see Figure S8, Supporting Information). Considering all available adsorption configurations for the three types, we end up with a total of 12 available states per single TAT molecule (see Figure 5a).

The observed molecular states allow for the realization of a particularly dense memory with the read-out speed limited by the scanning time it takes to evaluate the exact state of every single molecule. Higher speeds could be achieved by using units comprised of several interacting molecules, where the read-out is implemented as point measurement on only one molecule of a unit. We consider an elementary memory cell based solely on the low-bias switching of α-type TAT molecules (in the following referred to as active molecules). Here, transitions between the three states can be triggered by inelastic tunneling electrons (starting at about 60 mV for TAT in monolayers), whose energy is transformed into excitations of vibrational modes, which lead to a switch between the α_i configurations.[32,54] This enables switching rates of up to 10^3 Hz, i.e., it is solely limited by the time resolution of our STM electronics (0.5 ms). Moreover, at particular parameters, a pronounced switching directionality is observed for α-type TAT molecules within the honeycomb lattice (see Figure S9, Supporting Information), which allows for controlled driving of the system into a particular state. For the α-type system, we consider two possible scenarios – one active α-type molecule embedded into an inactive matrix composed of β- and γ-type (passive) neighboring molecules, as well as a medium composed of coupled α-type molecules. An STM image of the first scenario can be seen in Figure 5b, where an α-type molecule is surrounded by three β-type molecules. The $\Delta z(t)$-trace of the relative tip height shows three states as discussed above. The presence of adjacent β-type molecules imposes additional noise due to their fast two-level $\beta\leftrightarrow\beta'$ switching, which is simultaneously excited by the tunneling current; it is visible as a broadening of the main peaks in the histogram analysis of $\Delta z(t)$. A dense medium in this case would consist of a two-molecule unit with one active (α-type) and one passive (β- or γ-type) spacer molecule (see Figure S10, Supporting Information), which would yield a surface density of 2.6×10^{13} trit/cm^2, considering the unit cell area of 3.82 nm^2.

We now transform the β-type TAT at the bottom right into an α-type molecule (Figure 5c), which noticeably modifies the switching characteristics of the central read-out molecule. The coupling between both molecules leads to a superposition of switching levels on the read-out TAT molecule. Accordingly, the corresponding $\Delta z(t)$-trace clearly reveals nine well-separated states, whose occurrence suggests simultaneous excitation of the adjacent α-type TAT molecule due to hot carrier generation by the STM.[32,64] This behavior allows for the realization of a two-molecule unit with nine distinguishable states, that can be read out on a single molecule. Here, the medium would consist of units comprised of two active and two passive (spacer) TAT molecules (see Figure S10, Supporting Information). To expand this concept even further, we show in Figure 5d a configuration where all three neighboring molecules are transformed into the α-type. Taking into account all possible configurations of the four molecules, we expect to observe $3^4 = 81$ states. In our experiment, the $\Delta z(t)$-trace recorded over the central α-type molecule reveals 19 discernible states. Here, we only count the states which can be unambiguously identified in the dwell time diagram. However, we infer that more states are likely present. Particularly small jumps are difficult to assign due to the drift of the tunneling contact over long measurement periods. For the realized configuration, each unit cell comprises four active

**ADVANCED
SCIENCE NEWS**

www.advancedsciencenews.com

**ADVANCED
MATERIALS**

www.advmat.de
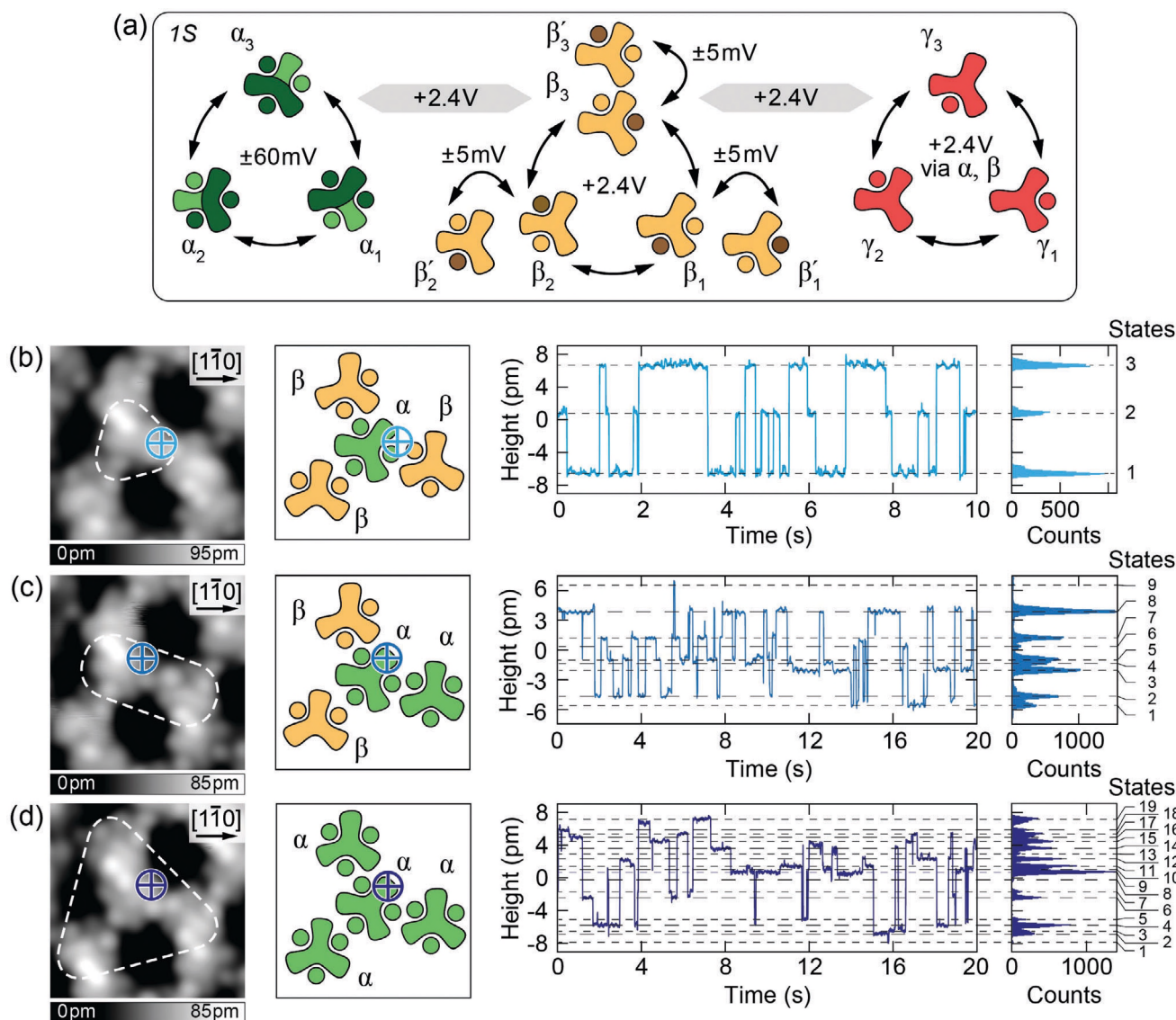
Figure 5. Multistate switching in interconnected TAT molecules. a) Pictograms representing the 12 discernible states of a TAT molecule on Ag(111). Upstanding ethyl groups are represented by circles. For the α-type molecules, the boomerang-shaped intensity within the molecules is highlighted by dark green. For the β-type molecules, the height variations of two ethyl groups upon two-state switching is visualized by the color change from yellow to brown. Arrows indicate switching processes with the corresponding threshold energies given. b–d) Topographic STM images (3.75×3.75 nm^2; $U = 10$ mV; $I = 100$ pA), corresponding pictograms of the molecular structures, as well as $\Delta z(t)$-traces of the low-bias switching and distribution histograms ($U = 100$ mV; $I = 100$ pA) for three configurations differing in the number of active neighbors of the central read-out α-type $3S$-TAT molecule. Configurations are highlighted by dashed lines. The lateral tip positions for each measurement are marked by crosses in STM images and in pictograms.

α-type molecules and two passive spacer molecules (Figure S10, Supporting Information). Although units with two and four active molecules provide a slight increase of the surface density, as can be seen from the active/passive ratio, the main advance lies in the possibility to use only one molecule of the unit for write/read-out operations, which reduces the access time. The average switching rates for the three studied units are very similar (see Figure S11, Supporting Information). However, an analysis in terms of the Allan deviation[65,66] shows that additional low-rate contributions are present for one-active- and three-active-neighbors configurations. Those can be assigned to the switching

of neighboring (one or three) active molecules, as the increasing distance from the electron injection point results in a reduction of the observed switching rate. This separation of switching rates in two (or more) groups is particularly appealing in terms of separate write/read-out operations on units comprised of several molecules. We note that the read out performance in our scheme is limited by the time resolution of the electronics, whereas the state separation in the sub-pm range is routinely achieved in up-to-date instrumentation. Thus, the high switching rates at relatively low bias voltages may result in fast memory operation times without any risks of damaging the arrays.

3. Conclusion

We have realized an ordered 2D network of ternary switching units represented by triazatruxene (TAT) molecules, organized in a honeycomb lattice on a Ag(111) surface. Using STM tip-induced high-bias pulses, applied to individual TAT molecules, we were able to reversibly manipulate their binding types – α, β, and γ. This allows us not only to program well-separated individual units composed of two or more interacting α-type molecules but also to expand the number of switching states for a single TAT molecule from three available for the low-bias switching of the α-type to overall twelve. Owing to the bias-dependent switching hierarchy and directionality, we achieve a high degree of control over the switching process, which, combined with a large number of accessible states, is unique to the best of our knowledge. Comparable molecular switches either lack the degree of control over the final state[57] or exhibit much fewer states.[56] Moreover, the reversible switching in a wide bias voltage range is demonstrated for individual molecules within densely packed molecular arrays. Additionally we show that the low-bias ternary switching of the most abundant α-type turns out to be strongly affected by the nearest neighbors. Owing to the high-bias switching, within the honeycomb lattice we are able to separate (program) units of two and four interacting α-type (active) TAT molecules, which show low-bias switching. For the tetrad, we observe 19 states, as measured on a read-out molecule, with a perspective to confine up to 81 distinct states. Based on our experiments, molecular-based memory units can be envisaged, although the wiring and in particular, room temperature operation would require further adaptation.

4. Experimental Section

N,N',N''-Triethyltriazatruxene was synthesized following a previously reported procedure.[67] The purity of the final material was verified by proton nuclear magnetic resonance spectroscopy and mass spectrometry (see Figure S12, Supporting Information). The surface of the Ag(111) single crystal (Surface Preparation Laboratory) was cleaned by repeated cycles of Ar$^+$ sputtering and subsequent annealing to about 890 K. Electrospray deposition of TAT molecules on the clean Ag(111) surface was performed as described elsewhere.[58,59] The sample was kept at room temperature during electrospray deposition, and then transferred into the cryogenic STM (Omicron Nanotechnology GmbH) operated at temperatures of 5–6 K. STM measurements were carried out in the constant-current mode using ground and polished PtIr tips (Nanoscore GmbH). The sign of the bias voltage corresponds to the potential at the sample.

DFT calculations were performed using the quantum chemistry code TURBOMOLE (version 7.1),[68] employing the def-SV(P) Gaussian basis set[69] and the Perdew–Burke–Ernzerhof (PBE) exchange–correlation functional.[70] In order to take van der Waals interactions into account, a dispersion correction to the PBE functional was employed.[71] Total energies were converged to a precision of better than 10^{-6} a.u., and geometry optimizations were carried out until the change of the maximum norm of the Cartesian gradient was below 10^{-5} a.u. A slab of three Ag layers was used as the substrate, in which the positions of the atoms in the upper two metal layers below the molecule were allowed to relax, while the bottom layer was held fixed at bulk lattice values.

Supporting Information

Supporting Information is available from the Wiley Online Library or from the author.

Conflict of Interest

The authors declare no conflict of interest.

Author Contributions

A.B. and T.B. contributed equally to this work. A.B., T.B., A.F., J.D., A.K.B., F. Paschke, and M.F. performed the experiments. A.B., T.B., O.Z., and M.F. analyzed the data. M.M., L.V., and R.F.W. performed the chemical synthesis and characterization. W.M.S., and F. Pauly performed the DFT calculations. M.F. conceptualized and supervised the project. M.F. drafted the manuscript. All authors discussed the results and contributed to writing the paper.

Competing Financial Interests

The authors declare no competing financial interests.

Data Availability Statement

The data that support the findings of this study are available from the corresponding author upon reasonable request.

[1] A. Aviram, M. A. Ratner, *Chem. Phys. Lett.* **1974**, *29*, 277.
[2] C. Joachim, J. K. Gimzewski, A. Aviram, *Nature* **2000**, *408*, 541.
[3] M. A. Ratner, *Nat. Nanotechnol.* **2013**, *8*, 378.
[4] D. Xiang, X. Wang, C. Jia, T. Lee, X. Guo, *Chem. Rev.* **2016**, *116*, 4318.
[5] T. A. Su, M. Neupane, M. L. Steigerwald, L. Venkataraman, C. Nuckolls, *Nat. Rev. Mater.* **2016**, *1*, 16002.
[6] H. Chen, J. F. Stoddart, *Nat. Rev. Mater.* **2021**, *6*, 804.
[7] S. J. van der Molen, P. Liljeroth, *J. Phys.: Condens. Matter.* **2010**, *22*, 133001.
[8] B. L. Feringa, W. R. Browne, *Molecular Switches*, Wiley-VCH, Weinheim **2011**.
[9] B. K. Pathem, Sh. A. Claridge, Y. B. Zheng, P. S. Weiss, *Annu. Rev. Phys. Chem.* **2013**, *64*, 605.
[10] J. K. Gimzewski, C. Joachim, R. R. Schlittler, V. Langlais, H. Tang, I. Johannsen, *Science* **1998**, *281*, 531.
[11] B. C. Stipe, M. A. Rezaei, W. Ho, *Science* **1998**, *279*, 1907.
[12] J. Michl, E. C. H. Sykes, *ACS Nano* **2009**, *3*, 1042.
[13] H. L. Tierney, C. J. Murphy, A. D. Jewell, A. E. Baber, E. V. Iski, H. Y. Khodaverdian, A. F. McGuire, N. Klebanov, E. C. H. Sykes, *Nat. Nanotechnol.* **2011**, *6*, 625.

[14] U. G. E. Perera, F. Ample, H. Kersell, Y. Zhang, G. Vives, J. Echeverria, M. Grisolia, G. Rapenne, C. Joachim, S.-W. Hla, *Nat. Nanotechnol.* **2013**, *8*, 46.

[15] H.-L. Lu, Y. Cao, J. Qi, A. Bakker, C. A. Strassert, X. Lin, K.-H. Ernst, Sh. Du, H. Fuchs, H.-J. Gao, *Nano Lett.* **2018**, *18*, 4704.

[16] Y. Zhang, J. P. Calupitan, T. Rojas, R. Tumbleson, G. Erbland, C. Kammerer, T. M. Ajayi, Sh. Wang, L. A. Curtiss, A. T. Ngo, S. E. Ulloa, G. Rapenne, S. W. Hla, *Nat. Commun.* **2019**, *10*, 3742.

[17] J. Homberg, M. Lindner, L. Gerhard, K. Edelmann, T. Frauhammer, Y. Nahas, M. Valášek, M. Mayor, W. Wulfhekel, *Nanoscale* **2019**, *11*, 9015.

[18] T. A. Balema, N. Ulumuddin, C. J. Murphy, D. P. Slough, Z. C. Smith, R. T. Hannagan, N. A. Wasio, A. M. Larson, D. A. Patel, K. Groden, J.-S. McEwen, Y.-S. Lin, E. C. H. Sykes, *J. Phys. Chem. C* **2019**, *123*, 23738.

[19] A. M. Larson, T. A. Balema, P. Zahl, A. C. Schilling, D. J. Stacchiola, E. C. H. Sykes, *ACS Nano* **2020**, *14*, 16558.

[20] I. Swart, T. Sonnleitner, J. Repp, *Nano Lett.* **2011**, *11*, 1580.

[21] S. Wickenburg, J. Lu, J. Lischner, H.-Z. Tsai, A. A. Omrani, A. Riss, C. Karrasch, A. Bradley, H. S. Jung, R. Khajeh, D. Wong, K. Watanabe, T. Taniguchi, A. Zettl, A. H. Castro Neto, S. G. Louie, M. F. Crommie, *Nat. Commun.* **2016**, *7*, 13553.

[22] N. Kocić, D. Blank, P. Abufager, N. Lorente, S. Decurtins, S.-X. Liu, J. Repp, *Nano Lett.* **2019**, *19*, 2750.

[23] M. Pörtner, Y. Wei, A. Riss, K. Seufert, M. Garnica, J. V. Barth, A. P. Seitsonen, L. Diekhöner, W. Auwärter, *Adv. Mater. Interfaces* **2020**, *7*, 2000080.

[24] H.-Z. Tsai, J. Lischner, A. A. Omrani, F. Liou, A. S. Aikawa, C. Karrasch, S. Wickenburg, A. Riss, K. C. Natividad, J. Chen, W.-W. Choi, K. Watanabe, T. Taniguchi, C. Su, S. G. Louie, A. Zettl, J. Lu, M. F. Crommie, *Nat. Electron.* **2020**, *3*, 598.

[25] P. Liljeroth, J. Repp, G. Meyer, *Science* **2007**, *317*, 1203.

[26] S. Pan, Q. Fu, T. Huang, A. Zhao, B. Wang, Y. Luo, J. Yang, J. Hou, *Proc. Natl. Acad. Sci. U. S. A.* **2009**, *106*, 15259.

[27] W. Auwärter, K. Seufert, F. Bischoff, D. Ecija, S. Vijayaraghavan, S. Joshi, F. Klappenberger, N. Samudrala, J. V. Barth, *Nat. Nanotechnol.* **2012**, *7*, 41.

[28] T. Kumagai, F. Hanke, S. Gawinkowski, J. Sharp, K. Kotsis, J. Waluk, M. Persson, L. Grill, *Nat. Chem.* **2014**, *6*, 41.

[29] G. J. Simpson, S. W. L. Hogan, M. Caffio, C. J. Adams, H. Früchtl, T. van Mourik, R. Schaub, *Nano Lett.* **2014**, *14*, 634.

[30] J. Kügel, A. Sixta, M. Böhme, A. Krönlein, M. Bode, *ACS Nano* **2016**, *10*, 11058.

[31] J. A. Garrido Torres, G. J. Simpson, C. J. Adams, H. A. Früchtl, R. Schaub, *Nano Lett.* **2018**, *18*, 2950.

[32] J. Kügel, M. Leisegang, M. Bode, *ACS Nano* **2018**, *12*, 8733.

[33] M. Leisegang, T. Zenger, M. Bode, J. Kügel, *J. Phys. Chem. C* **2020**, *124*, 10727.

[34] M. Leisegang, A. Christ, S. Haldar, S. Heinze, M. Bode, *Nano Lett.* **2021**, *21*, 550.

[35] B.-Y. Choi, S.-J. Kahng, S. Kim, H. Kim, H. W. Kim, Y. J. Song, J. Ihm, Y. Kuk, *Phys. Rev. Lett.* **2006**, *96*, 156106.

[36] V. Iancu, S.-W. Hla, *Proc. Natl. Acad. Sci. U. S.A.* **2006**, *103*, 13718.

[37] K. Scheil, T. G. Gopakumar, J. Bahrenburg, F. Temps, R. J. Maurer, K. Reuter, R. Berndt, *J. Phys. Chem. Lett.* **2016**, *7*, 2080.

[38] S. Jaekel, A. Richter, R. Lindner, R Bechstein, C. Nacci, S. Hecht, A. Kühnle, L. Grill, *ACS Nano* **2018**, *12*, 1821.

[39] R. Ohmann, L. Vitali, K. Kern, *Nano Lett.* **2010**, *10*, 2995.

[40] F. Mohn, J. Repp, L. Gross, G. Meyer, M. S. Dyer, M. Persson, *Phys. Rev. Lett.* **2010**, *105*, 266102.

[41] B. Borca, V. Schendel, R. Pétuya, I. Pentegov, T. Michnowicz, U. Kraft, H. Klauk, A. Arnau, P. Wahl, U. Schlickum, K. Kern, *ACS Nano* **2015**, *12*, 12506.

[42] F. Albrecht, S. Fatayer, I. Pozo, I. Tavernelli, J. Repp, D. Peña, L. Gross, *Science* **2022**, *377*, 298.

[43] L. Bogani, W. Wernsdorfer, *Nat. Mater.* **2008**, *7*, 179.

[44] E. Coronado, *Nat. Rev. Mater.* **2020**, *5*, 87.

[45] F. Prins, M. Monrabal-Capilla, E. A. Osorio, E. Coronado, H. S. J. van der Zant, *Adv. Mater.* **2011**, *23*, 1545.

[46] T. Miyamachi, M. Gruber, V. Davesne, M. Bowen, S. Boukari, L. Joly, F. Scheurer, G. Rogez, T. K. Yamada, P. Ohresser, E. Beaurepaire, W. Wulfhekel, *Nat. Commun.* **2012**, *3*, 938.

[47] T. Jasper-Toennies, M. Gruber, S. Karan, H. Jacob, F. Tuczek, R. Berndt, *Nano Lett.* **2017**, *17*, 6613.

[48] S. Johannsen, S. Schüddekopf, S. Ossinger, J. Grunwald, F. Tuczek, M. Gruber, R. Berndt, *J. Phys. Chem. C* **2022**, *126*, 7238.

[49] B. Zhang, F. Fan, W. Xue, G. Liu, Y. Fu, X. Zhuang, X.-H. Xu, J. Gu, R.-W. Li, Y. Chen, *Nat. Commun.* **2019**, *10*, 736.

[50] S. Goswami, S. P. Rath, D. Thompson, S. Hedström, M. Annamalai, R. Pramanick, B. R. Ilic, S. Sarkar, S. Hooda, C. A. Nijhuis, J. Martin, R. S. Williams, S. Goswami, T. Venkatesan, *Nat. Nanotechnol.* **2020**, *15*, 380.

[51] S. Wagner, F. Kisslinger, S. Ballmann, F. Schramm, R. Chandrasekar, T. Bodenstein, O. Fuhr, D. Secker, K. Fink, M. Ruben, H. B. Weber, *Nat. Nanotechnol.* **2013**, *8*, 575.

[52] C. Zhou, X. Li, Z. Gong, C. Jia, Y. Lin, C. Gu, G. He, Y. Zhong, J. Yang, X. Guo, *Nat. Comm.* **2018**, *9*, 807.

[53] J. Li, S. Hou, Y.-R. Yao, C. Zhang, Q. Wu, H.-C. Wang, H. Zhang, X. Liu, C. Tang, M. Wei, W. Xu, Y. Wang, J. Zheng, Z. Pan, L. Kang, J. Liu, J. Shi, Y. Yang, C. J. Lambert, S.-Y. Xie, W. Hong, *Nat. Mater.* **2022**, *21*, 917.

[54] A. Bauer, M. Maier, W. M. Schosser, J. Diegel, F. Paschke, Yu. Dedkov, F. Pauly, R. F. Winter, M. Fonin, *Adv. Mater.* **2020**, *32*, 1907390.

[55] L. Vogelsang, T. Birk, F. Paschke, A. Bauer, V. Enenkel, L. M. Holz, M. Fonin, R. F. Winter, *Inorg. Chem.* **2023**, *62*, 16236.

[56] T. Huang, J. Zhao, M. Feng, A. A. Popov, S. Yang, L. Dunsch, H. Petek, *Nano Lett.* **2011**, *11*, 5327.

[57] H. J. Chandler, M. Stefanou, E. E. B. Campbell, R. Schaub, *Nat. Commun.* **2019**, *10*, 2283.

[58] Ph. Erler, P. Schmitt, N. Barth, A. Irmler, S. Bouvron, T. Huhn, U. Groth, F. Pauly, L. Gragnaniello, M. Fonin, *Nano Lett.* **2015**, *15*, 4546.

[59] L. Gragnaniello, F. Paschke, Ph. Erler, P. Schmitt, N. Barth, S. Simon, H. Brune, S. Rusponi, M. Fonin, *Nano Lett.* **2017**, *17*, 7177.

[60] B. Yang, Y. Wang, H. Cun, S. Du, M. Xu, Y. Wang, K.-H. Ernst, H.-J. Gao, *J. Am. Chem. Soc.* **2010**, *132*, 10440.

[61] D. X. Shi, J. Ji, X. Lin, X. B. He, J. C. Lian, L. Gao, J. M. Cai, H. Lin, S. X. Du, F. Lin, C. Seidel, L. F. Chi, W. A. Hofer, H. Fuchs, H.-J. Gao, *Phys. Rev. Lett.* **2006**, *96*, 226101.

[62] N. Hauptmann, K. Scheil, T. G. Gopakumar, F. L. Otte, C. Schütt, R. Herges, R. Berndt, *J. Am. Chem. Soc.* **2013**, *135*, 8814.

[63] C. Thiele, L. Gerhard, T. R. Eaton, D. M. Torres, M. Mayor, W. Wulfhekel, H. v. Löhneysen, M. Lukas, *New J. Phys.* **2015**, *17*, 053043.

[64] J. N. Ladenthin, L- Grill, S. Gawinkowski, S. Liu, J. Waluk, T. Kumagai, *ACS Nano* **2015**, *9*, 7287.

[65] D. W. Allan, *Proc. IEEE* **1966**, *54*, 221.

[66] G. Margiani, S. Guerrero, T. L. Heugel, C. Marty, R. Pachlatko, T. Gisler, G. D. Vukasin, H.-K. Kwon, J. M. L. Miller, N. E. Bousse, T. W. Kenny, O. Zilberberg, D. Sabonis, A. Eichler, *Appl. Phys. Lett.* **2022**, *121*, 164101.

[67] L. Ji, Q. Fang, M.-S. Yuan, M.-Z.-G. Liu, Y.-X. Shen, H.-F. Chen, *Org. Lett.* **2010**, *12*, 5192.

[68] S. G. Balasubramani, G. P. Chen, S. Coriani, M. Diedenhofen, M. S. Frank, Y. J. Franzke, F. Furche, R. Grotjahn, M. E. Harding, C. Hättig, A. Hellweg, B. Helmich-Paris, C. Holzer, U. Huniar, M. Kaupp, A. M.

2401662 (9 of 10)

**ADVANCED
SCIENCE NEWS**

www.advancedsciencenews.com

**ADVANCED
MATERIALS**

www.advmat.de

Khah, S. K. Khani, T. Müller, F. Mack, B. D. Nguyen, S. M. Parker, E. Perlt, D. Rappoport, K. Reiter, S. Roy, M. Rückert, G. Schmitz, M. Sierka, E. Tapavicza, D. P. Tew, et al., *J. Chem. Phys.* **2020**, *152*, 184107.

[69] A. Schäfer, H. Horn, R. Ahlrichs, *J. Chem. Phys.* **1992**, *97*, 2571.

[70] J. P. Perdew, *Phys. Rev. B* **1986**, *33*, 8822.

[71] S. Grimme, *J. Comput. Chem.* **2004**, *25*, 1463.